

Galaxy groups in the 2dFGRS: the number density of groups

V.R. Eke¹, Carlton M. Baugh¹, Shaun Cole¹, Carlos S. Frenk¹, Julio F. Navarro^{2,*}

¹*Department of Physics, University of Durham, South Road, Durham DH1 3LE, UK*

²*Department of Physics and Astronomy, University of Victoria, Victoria, BC, V8P 5C2, Canada*

11 September 2018

ABSTRACT

The abundance of galaxy clusters as a function of mass is determined using the 2dFGRS Percolation-Inferred Galaxy Group (2PIGG) catalogue. This is used to estimate the amplitude of the matter fluctuation spectrum, parametrised by the linear theory rms density fluctuations in spheres of $8h^{-1}$ Mpc, σ_8 . The best-fitting value for this parameter is highly correlated with the mean matter density in the Universe, Ω_m , and is found to satisfy $\sigma_8 = 0.25 \Omega_m^{-0.92-4.5(\Omega_m-0.22)^2} \pm 10\%$ (statistical) $\pm 20\%$ (systematic) for $0.18 \leq \Omega_m \leq 0.50$, assuming that $\Omega_m + \Omega_\Lambda = 1$. This gives $\sigma_8 = 0.89$ when $\Omega_m = 0.25$. A ~ 20 per cent correction has been applied to undo the systematic bias inherent in the measurement procedure. Mock catalogues, constructed from large cosmological N-body simulations, are used to help understand and model these systematic errors. The abundance of galaxy groups as a function of group b_J band luminosity is also determined. This is used in conjunction with the halo mass function, determined from simulations, to infer the variation of halo mass-to-light ratio over four orders of magnitude in halo mass. The mass-to-light ratio shows a minimum value of $100hM_\odot/L_\odot$ in the b_J band at a total group luminosity of $L_{b_J} \approx 5 \times 10^9 h^{-2} L_\odot$. Together with the observed Tully-Fisher relation, this implies that the observed rotation speed of Tully-Fisher galaxies is within ~ 10 per cent of the typical circular speed of haloes hosting brightest galaxies of the same luminosity.

Key words: galaxies: groups – galaxies: haloes – galaxies: clusters: general – large-scale structure of Universe.

1 INTRODUCTION

The abundance of galaxy clusters provides a very direct way to estimate σ_8 , the linear theory rms density fluctuations in comoving spheres of $8h^{-1}$ Mpc, extrapolated to redshift zero (e.g. Peebles, Daly & Juskiewicz 1989; Frenk et al. 1990; White, Efstathiou & Frenk 1993; Eke, Cole & Frenk 1996; Viana & Liddle 1996; Ikebe et al. 2002; Pierpaoli et al. 2003; Schuecker et al. 2003; Henry 2004). This parameter sets the normalisation of the matter power spectrum. As the cluster abundance varies rapidly with σ_8 , the main difficulty in this method is not the determination of the abundance, but knowing the mass of the objects under consideration. The current ~ 10 per cent uncertainty on the value of σ_8 (see Viana et al. 2003 and Henry 2004 for recent discussions of cluster-based estimates) brackets important differences in the formation histories of dark matter haloes. This has

implications for a broad range of topics, such as the redshift at which gravitationally bound structures first form, the merger histories of galaxy-sized haloes and the concentration of the dark matter density profile within haloes.

Many of the cluster samples used so far to determine σ_8 have been based on the ROSAT X-ray All Sky Survey. It is clearly desirable to supplement these estimates with others derived from independent cluster samples, where the clusters are found using different techniques. There are already a number of studies that have estimated the galaxy cluster mass function using catalogues of optically selected objects (e.g. Bahcall & Cen 1993; Biviano et al. 1993; Girardi et al. 1998; Martínez et al. 2002; Bahcall et al. 2003). In this study, the 2dFGRS Percolation-Inferred Galaxy Group (2PIGG) catalogue (Eke et al. 2004a) is used, in conjunction with mock galaxy catalogues, to provide a new estimate of the mass function. The use of mock catalogues extends the previous work by quantifying some of the systematic biases inherent in the method.

* CIAR and Guggenheim Fellow

The group luminosity function, that is the abundance of groups as a function of their total luminosity, has previously been determined using galaxy redshift survey data by Moore, Frenk & White (1993), Marinoni, Hudson & Giuricin (2002) and Martínez et al. (2002). The 2PIGG catalogue increases the number of available groups by a factor of approximately two relative to the work of Martínez et al. (2002), who used the earlier data release from the 2dFGRS. The group luminosity function provides an indirect way to measure the mass function if one knows how to relate mass to luminosity. For instance, if the statistical uncertainties on the cluster dynamical mass estimates are significantly larger than those on the cluster luminosities, then the combination of the group luminosity function with a typical cluster mass-to-light ratio will yield a more accurate estimation of the cluster mass function than would be found from directly using the dynamical masses. Turning this around, given a theoretical mass function and a measured group luminosity function, one can infer the mapping from mass to luminosity as a function of group size (Marinoni & Hudson 2002). This picks out the group scales at which mass is most efficiently turned into starlight and, as such, encodes important clues about the process of galaxy formation (Benson et al. 2000; van den Bosch, Yang & Mo 2003).

In this paper, mock galaxy catalogues, constructed from N-body simulations of the Λ CDM cosmology combined with a semi-analytical model for placing galaxies into dark matter haloes, are used to estimate how group-finding in the 2dFGRS leads to biases in the recovered cluster mass and group luminosity functions. Then the 2PIGG catalogue is used to estimate the cluster mass and group luminosity functions, and the mass-to-light ratio for groups. This final quantity is inferred under the assumption that the group mass function is given by the fit to the halo mass function measured in N-body simulations, as described by Jenkins et al. (2001, J01). Given the typical halo mass, or equivalently circular speed, at a given luminosity, one can compare these results with the observed Tully-Fisher relation (Tully & Fisher 1977; Bell & de Jong 2001). Under the assumption that observed Tully-Fisher galaxies lie in typical haloes, this determines the conversion from observed rotation speeds of galaxies to halo circular velocities. This result has some bearing on the long-running debate concerning the ability of galaxy formation models to match the galaxy luminosity function and the Tully-Fisher relation simultaneously (Kauffmann, White & Guiderdoni 1993; Cole et al. 1994; Heyl et al. 1995).

Section 2 contains a brief description of the mock and real catalogues used in this study. The mass function calculation and the constraint this imposes upon σ_8 is described in Section 3. Section 4 contains the group luminosity function results, which are applied to determining the group mass-to-light ratio variation in Section 5. In Section 6, the halo mass-to-light ratios are compared with the observed Tully-Fisher relation.

2 BRIEF DESCRIPTION OF THE MOCK AND REAL CATALOGUES

The construction of the 2PIGG catalogue is described in detail by Eke et al. (2004a). This paper also discusses the generation of mock galaxy catalogues from a combination of

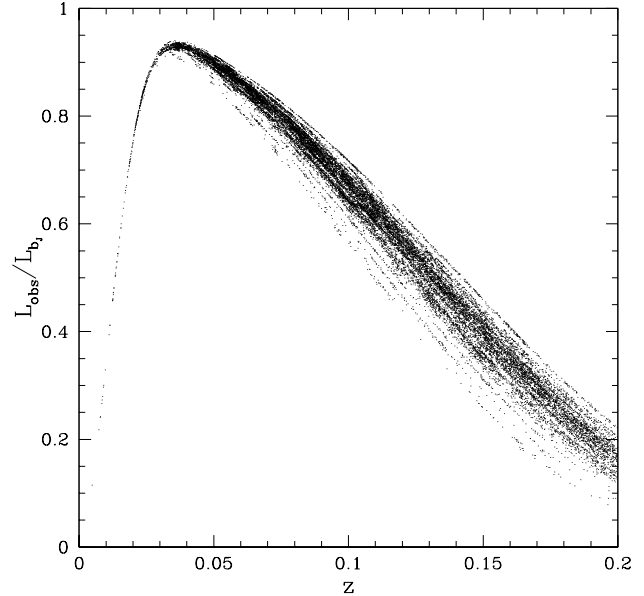


Figure 1. The ratio of observed to total group luminosity for each mock group as a function of redshift. The total group luminosity is estimated using the global galaxy luminosity Schechter function described in the text to correct for galaxies outside the 2dFGRS flux limits.

dark matter N-body simulations and semi-analytical galaxy formation models. The catalogue has been constructed from the two contiguous patches in the 2dFGRS (Colless et al. 2001), which contain a total of $\sim 190\,000$ galaxies. Of these, about 55 per cent are placed into $\sim 29\,000$ groups containing at least two members. The median redshift of the groups is 0.11, like that of the galaxies, and the reliability of the estimated group masses and luminosities has been gauged using mock catalogues as described by Eke et al. (2004b).

Mocks have been created from N-body simulations of the standard Λ CDM model with parameter values $\Omega_m = 0.3$, $\Omega_\Lambda = 0.7$ and $\sigma_8 = 0.90$ and 0.71 . The $\sigma_8 = 0.90$ simulation is the Λ CDM2 run described by Jenkins et al. (1998), whereas the lower σ_8 simulation cube contains 288^3 particles in a box of length $154h^{-1}$ Mpc, corresponding to a very similar mass resolution. Both the semi-analytical models of Cole et al. (2000) and Benson et al. (2003) have been used to place galaxies into the dark matter distributions in the two simulation cubes. Note that the luminosities of the semi-analytical mock galaxies have been scaled by small, colour-preserving amounts so that the mock galaxy b_J -band luminosity function exactly matches that found in the 2dFGRS. Dynamical masses of groups are estimated using

$$M = A \frac{\sigma^2 r}{G}, \quad (2.1)$$

where $A = 5$ (Eke et al. 2004a), σ is the 1-dimensional velocity dispersion, calculated using the gapper algorithm (Beers, Flynn & Gebhardt 1990) and removing 85 km s^{-1} in quadrature to account for redshift measurement errors, and r is the *r.m.s.* projected separation of galaxies from the group centre, assuming an $\Omega_m = 0.3$, $\Omega_\Lambda = 0.7$ cosmological model. Observed group luminosities are estimated by summing the

luminosities of the individual galaxies with their associated weights to account for spectroscopic incompleteness:

$$L_{\text{obs}} = \sum_i^N w_i L_i. \quad (2.2)$$

This observed group luminosity is then corrected for galaxies lying outside the survey flux limits assuming a global Schechter galaxy luminosity function

$$\phi(L)dL = \phi_* \left(\frac{L}{L_*}\right)^\alpha \exp\left(-\frac{L}{L_*}\right) \frac{dL}{L_*}, \quad (2.3)$$

with $(M_* - 5\log_{10} h, \alpha) = (-19.725, -1.18)$ (Eke et al. 2004b) and $M_\odot = 5.33$ in the b_J band. Fig. 1 shows the ratio of L_{obs} to the total group luminosity, L_{b_J} . Note that there are upper and lower flux limits imposed on the galaxies in the 2dFGRS, hence the shape traced out by the galaxy groups in Fig. 1, with the upper flux limit rejecting bright galaxies in the nearby groups, and the lower flux limit being important at higher redshifts. The stripes traced out by the points are a result of the distinct flux limits in different patches of the survey.

In all of what follows, the group sample will be restricted to the $z < 0.12$ objects, because at higher redshifts, less than half of the total group luminosity is contained in visible galaxies and the correction for this missing light becomes too uncertain (see Fig. 1). For the same reason, the volume at $z < 0.02$ will also be excised.

When calculating the abundance of groups, it is necessary to know the volume surveyed. The maximum volume within which a particular group could have been detected by a survey is V_{max} . If a group is defined to comprise at least N galaxies, then the group V_{max} could be approximated by the V_{max} of the N th most luminous galaxy in that group. This takes into account the variable sky coverage as a function of flux in the 2dFGRS. However, for $N > 1$, this ignores the possibility that the set of galaxies linked together by the friends-of-friends (FOF) algorithm may not remain grouped at different redshifts, when the linking volume has changed in size and the set of galaxies satisfying the flux limits of the survey may have changed to the extent that parts of the group are no longer joined. To deal with these issues exactly would be awkward. These complications are minor though, because the linking volume changes with redshift to take into account the varying sampling of the galaxy distribution. Consequently, the V_{max} of the N th most luminous galaxy is used to define the group V_{max} throughout the rest of this paper. The mock catalogues can be used to gauge the extent to which this choice biases the results. Of course, for the group luminosity function, $N_{\text{min}} = 1$ can be used, in which case the V_{max} value is correct.

3 CLUSTER MASS FUNCTIONS

The accuracy with which dynamical masses can be estimated varies rapidly with the number of galaxies sampling the group potential (see figure 3 of Eke et al. 2004b). Errors in estimated masses coupled with the steep decline in the abundance of clusters, i.e. groups with masses above $\sim 10^{14} h^{-1} M_\odot$, as a function of increasing mass, lead to systematic biases in the inferred abundance of clusters. This happens because more low-mass objects are scattered to higher masses than are scattered down from those higher

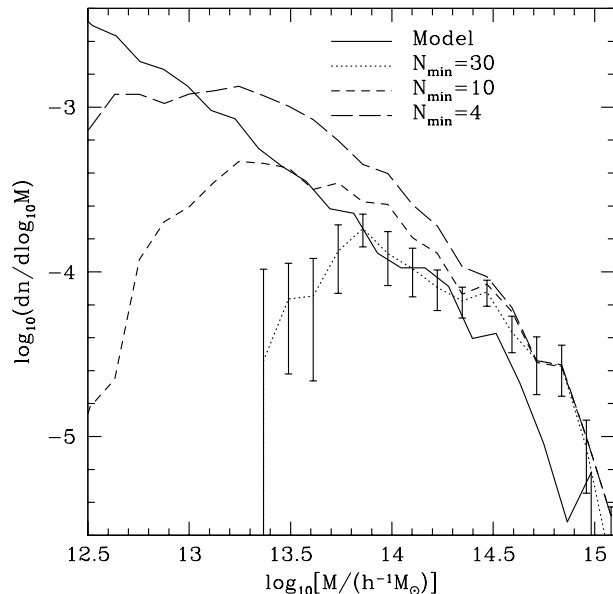


Figure 2. Model and mock recovered mass functions. The solid line traces the mass function of dark matter haloes in the simulation cube (the Λ CDM2 run by Jenkins et al. 1998). The other lines show the mass function inferred using different minimum numbers of galaxies to define the group sample, as indicated in the key. Statistical errors, shown by the error bars, are calculated using the scatter between 22 mock catalogues constructed from the Hubble Volume simulation.

masses. Consequently, the abundance of high mass galaxy clusters will be systematically overestimated as a result of the uncertainties in measuring the individual cluster masses. This effect is shown in Fig. 2 for the mock catalogues, which compares the mass functions recovered from groups samples of different N_{min} at $z \leq 0.12$ with the mass function of dark matter haloes in the simulation cube. The model mass function shows the abundance of dark matter haloes found using a friends-of-friends (FOF) group-finder with a linking length $b = 0.2$ times the mean interparticle separation (Davis et al. 1985). Error bars represent the standard deviation among the results from 22 different mock catalogues made using the Hubble Volume simulation (Evvard et al. 2002). Norberg et al. (2002) provide a detailed description of how the mock catalogues are constructed. Hawkins et al. (2003) have shown that the galaxies in mock catalogues made from the Hubble Volume simulation cluster like those in the 2dFGRS, suggesting that the use of these mocks is appropriate. Cosmic variance only increases the statistical errors by ~ 10 per cent relative to the $1/V_{\text{max}}$ -weighted Poisson errors. Note that restricting the sample to include only groups containing large numbers of galaxies introduces incompleteness at lower masses, which, to some extent, counteracts the overestimation of the mass function due to mass measurement errors. Nevertheless, as Fig. 2 shows, the abundance is still overestimated by a factor of ~ 2 for $M \gtrsim 3 \times 10^{14} h^{-1} M_\odot$. For the remainder of this Section, $z_{\text{max}} = 0.12$ and $N_{\text{min}} = 20$ will be used. These cuts restrict the sample to ~ 350 clusters.

The dynamically-inferred group masses show more scat-

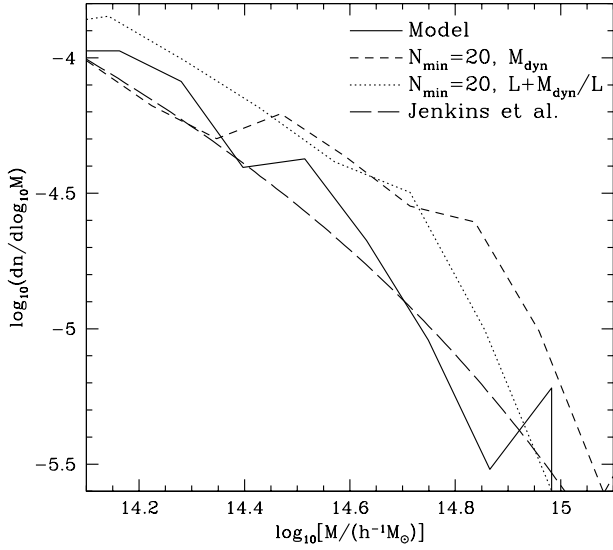


Figure 3. Mass functions for dark haloes in the simulation and for groups identified in the mock catalogue. A solid line traces the mass function of dark matter haloes in the simulation cube. Also plotted are mass functions for mock groups inferred using dynamical masses (short-dashed line) and group luminosities with a shift for the typical mass-to-light ratio (dotted line). The long-dashed line represents the J01 fitting formula to describe the dark matter halo mass function appropriate for the power spectrum of the model.

ter about the true halo mass in the simulations than masses inferred using the total group luminosity and a typical mass-to-light ratio (Eke et al. 2004b). Thus, one can produce a more robust estimate of the cluster mass function by using the cluster total luminosity function and a typical mass-to-light ratio. This is shown, at least for the highest masses, in Fig. 3. The median mass-to-light ratio for all mock groups with $L > 10^{11.5} h^{-2} L_{\odot}$ ($\Upsilon = 471 h M_{\odot}/L_{\odot}$) has been used as a global shift to the cluster luminosity function to infer the mass function (dotted line). The mass-to-light ratio varies little for these most massive objects (Eke et al. 2004b), so this simple shift is appropriate. Also shown is the J01 fitting formula for the mass function that describes the population of haloes from which the model curve is sampled. Hereafter in this paper, only recovered mass functions obtained using the cluster luminosity function and the cluster mass-to-light ratio, as shown by the dotted line in Fig. 3, will be considered.

In order to place constraints upon the normalisation of the power spectrum, it is necessary firstly to model the bias in recovering the mass function and secondly to compare the measured mass function in the 2PIGG catalogue with the biased models for each value of σ_8 . Fig. 4 shows the J01 mass functions for two different values of σ_8 , before and after applying a shift to account for the measurement errors. An approximation to the bias introduced by measuring the mass function is to translate the J01 curves to the right by 0.17 and 0.20 for $\sigma_8 = 0.90$ and 0.71 respectively. These shifts provide the best χ^2 fits (assuming weighted Poisson

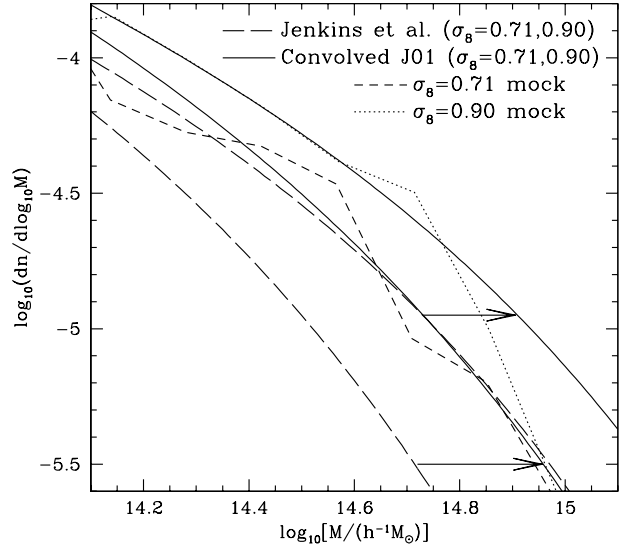


Figure 4. The σ_8 dependence of the recovered mass function. Long-dashed lines show the J01 fitting function describing the mass function for the two different values of σ_8 used to make mock catalogues. The solid lines show the effect of measurement errors on these curves, as described in the text. A dotted line traces the mass function recovered from the $\sigma_8 = 0.90$ mock, whereas the short-dashed line is the corresponding curve for $\sigma_8 = 0.71$. The horizontal arrows show the impact of the measurement bias.

errors) to the mass functions measured from the mock group catalogues for both values of σ_8 . The uncertainty on the size of these translations, judging by the change in χ^2 of the resulting fits, is ~ 7 per cent in mass for the Cole et al. (2000) mocks. The shifts required for the mocks made using the Benson et al. (2003) semi-analytical procedure differ by ~ 7 per cent from the Cole et al. (2000) mocks. Thus, one should consider these corrections to be uncertain by ~ 10 per cent in mass. With these shifts, each model curve can be converted into a mass function in measurement space. Note how the measurement bias is larger for the lower value of σ_8 , where the clusters are more difficult to detect because of the lower contrast. This, unfortunately, reduces the power of the test, but it is nevertheless apparent that these two different values of σ_8 can still be distinguished.

The mass functions inferred from the 2PIGG data are shown in Fig. 5. Once again, the directly determined mass function, based on dynamical masses, gives higher abundances at this mass than the mass function recovered from the luminosity function and the typical cluster mass-to-light ratio ($\Upsilon = 429 h M_{\odot}/L_{\odot}$). Note that the 2PIGG results generally lie between the convolved model curves for $\sigma_8 = 0.71$ and 0.90 ($\Omega_m = 0.3$ in both cases). Error bars again are the $1/V_{\max}$ -weighted Poisson errors. This neglects the ~ 10 per cent additional contribution from cosmic variance, which is minor relative to the systematic uncertainties inherent in this method.

By assuming that the convolving function generates a mean shift that varies linearly with σ_8 and not at all with Ω_m , one can extrapolate the convolved model to a range

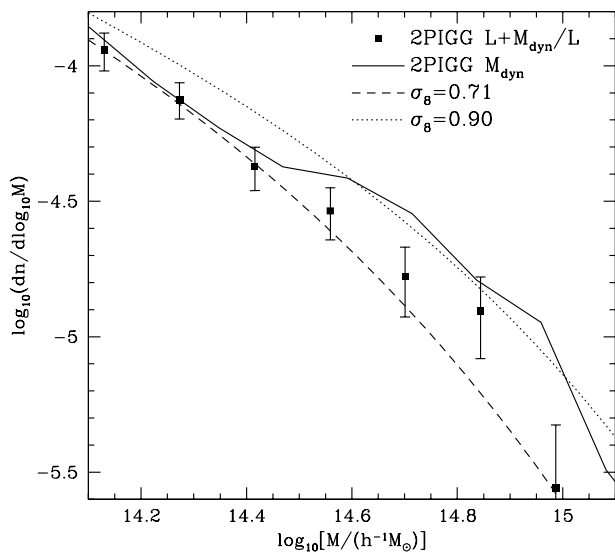


Figure 5. 2PIGG and model group mass functions. The model mass functions after convolution with the measurement errors, shown with solid lines in the previous figure, are now shown with dotted ($\sigma_8 = 0.90$) and dashed ($\sigma_8 = 0.71$) lines. The points with error bars show the 2PIGG results using the cluster luminosity function and typical mass-to-light ratio. A solid line shows the 2PIGG mass function based on the dynamical mass measurements of equation 2.1.

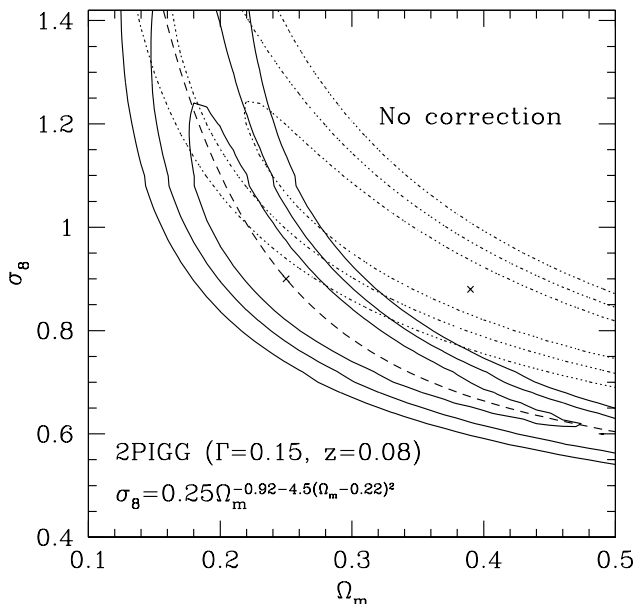


Figure 6. The constraints on σ_8 and Ω_m from the 2PIGG catalogue. The χ^2 contours are shown, with (solid lines) and without (dotted lines) the correction for the bias in the recovery of the mass function. The contours contain 68, 95 and 99.7 per cent of probability, and a cross marks the best-fitting parameter set for each case. The dashed line shows a fit to the most probable $\sigma_8(\Omega_m)$ for the bias-corrected contours.

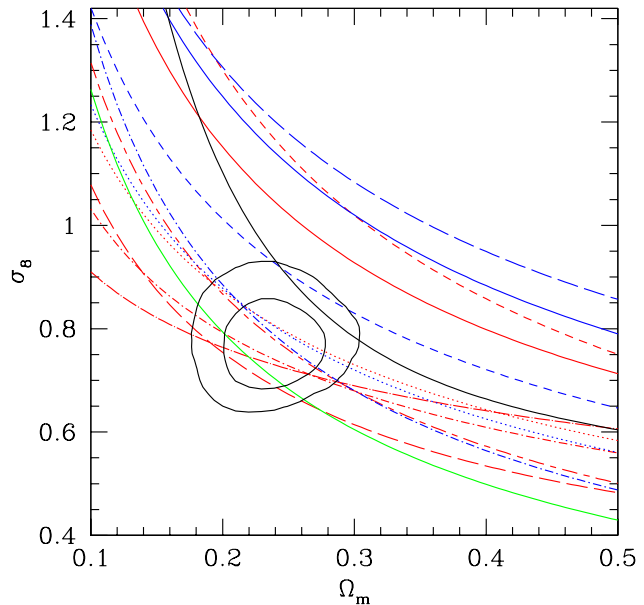


Figure 7. Comparison of the 2PIGG results (solid black line) with various other estimates of the amplitude of matter fluctuations. The red lines show measurements based largely on the cluster abundance: Eke, Cole & Frenk (1996, solid line); Pierpaoli et al. (2001, short dashed); Bahcall et al. (2003, short-long dashed); Reiprich & Böhringer (2002, dot-short dashed); Seljak (2002, dotted); Viana, Nichol & Liddle (2002, long dashed); Allen et al. (2003, dot-long dashed). Blue lines trace the amplitudes inferred using weak lensing-based estimates from: Brown et al. (2003, dotted); Rhodes et al. (2004, long dashed); Heymans et al. (2005, dot-short dashed); Massey et al. (2005, solid); van Waerbeke, Mellier & Hoekstra (2005, short dashed). The green line shows the results of Tinker et al. (in preparation), who use a model of the halo occupation distribution, in conjunction with the galaxy correlation functions for different luminosity galaxies in the 2dFGRS and the 2PIGG mass-to-light ratio variation with group size. The rounded 68 and 95 per cent probability contours are from figure 12 of Sanchez et al. (2005), and result from a joint analysis of the power spectra of both the CMB and 2dFGRS.

of Ω_m and σ_8 , in order to determine the best-fitting values of these parameters. The results of this exercise are shown in Fig. 6. Only the 5 data points with $14.4 \leq \log[M/(h^{-1} M_\odot)] \leq 15$ are used in the χ^2 fit. The contours contain 68, 95 and 99.7 per cent of the probability. Dotted and solid lines show the constraints on the parameters before and after the correction for the measurement bias is applied. In short, this correction changes the best-fitting parameters from $(\Omega_m = 0.39, \sigma_8 = 0.88)$ to $(0.25, 0.90)$. The dashed line showing the variation of the best-fitting σ_8 as a function of Ω_m in the range $0.18 \leq \Omega_m \leq 0.50$ has the equation:

$$\sigma_8 = 0.25\Omega_m^{-0.92-4.5(\Omega_m-0.22)^2}. \quad (3.1)$$

Note that these contours have all been calculated under the assumption that the CDM transfer function has a shape given by $\Gamma = 0.15$ (Bardeen et al. 1986; Sugiyama 1995) as has recently been measured using the 2dFGRS (Cole et al. 2005). Using values of $\Gamma = 0.1$ or 0.25 changes the value of σ_8 by less than 5 per cent for $\Omega_m = 0.3$. While the statistical uncertainty upon the estimate of $\sigma_8(\Omega_m)$ is small (~ 10 per

cent), the systematic correction that has been applied to account for the measurement bias is substantially bigger (~ 20 per cent). It is worthwhile reiterating that the probability contours involve extrapolating the noisy fits of convolving functions to the mock recovered mass functions, so this systematic shift is quite rough. As was discussed above, the correction is uncertain by ~ 10 per cent in mass. This corresponds roughly to 5 per cent systematic uncertainty in the estimated σ_8 value from this shift. There is another systematic uncertainty associated with the calibration of the mass estimation (the value of A in equation 2.1).

An illustration of the relative importance of systematic uncertainties in current estimates of σ_8 is contained in Fig. 7, which shows the results from a number of different studies. The 2PIGG line is shown in black, along with other cluster abundance-based estimates in red, and weak lensing-based results in blue. The black probability contours show the results of Sanchez et al. (2005), who jointly analysed the CMB and 2dFGRS power spectra. The green line shows the best-fitting parameters inferred using the 2dFGRS correlation functions, a model for the halo occupation distribution and the 2PIGG mass-to-light ratios (Tinker et al., private communication). Quoted errors on the various curves are usually of the order of 10 – 15 per cent. Some of the variation from one study to another will come from assuming different power spectrum shapes (Γ), but this dependence is quite weak (Seljak 2002; Rhodes et al. 2004) so the excess scatter between the curves is a sign of other systematic effects. For the cluster abundance-based measurements, the main source of systematic differences comes due to the choice of the mass-observable relation (see Henry 2004).

4 GROUP TOTAL LUMINOSITY FUNCTION

The total b_J -band group luminosity function is a distribution that, unlike the galaxy luminosity function, can readily be compared with theoretical dark matter halo mass functions. In Section 5 the group luminosity function will be used in conjunction with theoretical mass functions to derive halo mass-to-light ratios.

Fig. 8 shows how well the b_J -band group luminosity function can be recovered from a mock catalogue. Only the groups with $0.02 \leq z \leq 0.07$ are included in the calculation of these curves. As the upper limit in redshift is increased, the typical correction for luminosity in galaxies fainter than the flux limit increases. Consequently, the recovered luminosity functions become increasingly biased high. On the other hand, if the maximum redshift is too restrictive, then there are insufficient clusters, and the volume probed may no longer be representative of the Universe as a whole. The choice of $z_{\max} = 0.07$ is a compromise between these two competing factors. Even with this value, the group luminosity function recovered from the mock catalogue is still biased slightly high relative to the true model function for the most luminous systems in the simulation. Note how the value of N_{\min} impacts upon the abundance of low luminosity groups. The best recovery of the model occurs when $N_{\min} = 1$. Some depletion of the less luminous groups is evident: these objects sometimes contaminate the bigger groups, causing the abundance of the more luminous systems to be slightly over-estimated.

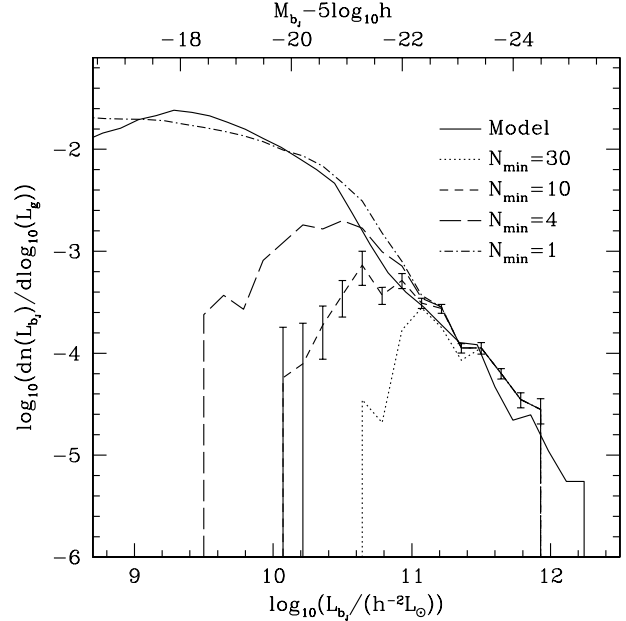


Figure 8. The abundance of groups as a function of their total b_J -band luminosity. A solid line traces the actual group luminosity function in the simulation, and the other lines show the recovered functions using all mock groups with $z < 0.07$ and $N \geq N_{\min}$. Error bars are shown only for the $N_{\min} = 10$ case, and are calculated using the scatter between 22 different mocks made from the Hubble Volume simulation.

Fig. 9 shows how the group luminosity function recovered from the 2PIGG catalogue compares with that in a mock catalogue constructed from a simulation with $\sigma_8 = 0.9$ using the Cole et al. (2000) semi-analytical model. Only groups at $z \leq 0.07$ that contain at least one detectable galaxy are included in the calculation. The 2PIGG results accurately trace those recovered from the mock. Also shown is the 2dFGRS galaxy luminosity function, which crosses the group luminosity function at $\sim L_*$, the characteristic luminosity in the galaxy luminosity function (Norberg et al. 2002). Many of the fainter galaxies reside in groups with $L > L_*$; hence the abundance of low luminosity groups lies beneath that of the galaxies.

Fig. 10 shows how the 2PIGG results compare with other published work. The group luminosity functions of Marinoni et al. (2002), from the Nearby Optical Galaxy (NOG) catalogue, Moore, Frenk & White (1993), from the CfA survey, and Martínez et al. (2002), using the 2dF Galaxy Group Catalogue (2dFGGC), are all quite similar to that from the 2PIGGs for group luminosities above $\sim 10^{11} h^{-2} L_\odot$. At lower luminosities, the 2dFGGC results lie lower, because of the requirement that their groups contain at least 4 galaxies. The 2PIGG group luminosity function also lies somewhat above those of Moore et al. and Marinoni et al. Note that the Marinoni et al. curve has been shifted 0.55 magnitudes fainter from their published fit to account for both the 0.3 magnitudes difference between their B band (RC3 asymptotic photometric system) and b_J (Marinoni, private communication), and 0.25 magnitudes of internal absorption that they had included. The Moore et al. curve has been shifted under the assumption

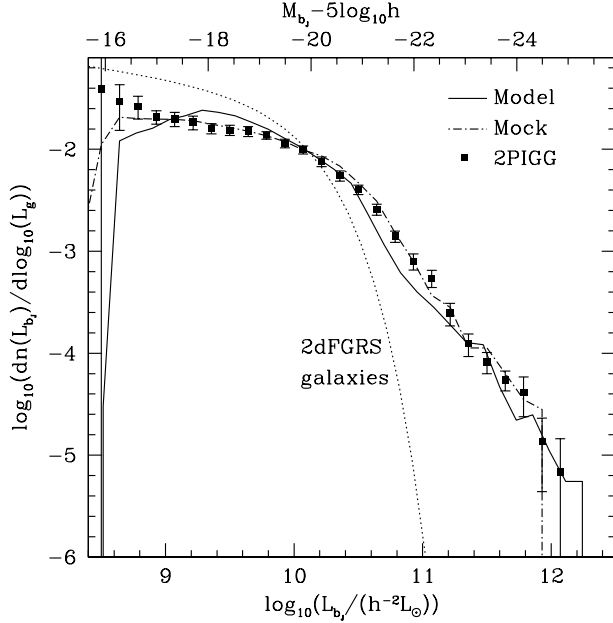


Figure 9. The abundance of groups as a function of their total b_J -band luminosity. A solid line traces the model group luminosity function, the dot-dashed line shows the recovered function using all mock groups with $z < 0.07$ and $N \geq 1$. The points show the group luminosity function found using the 2PIGG catalogue.

that $b_J = B_{\text{Zwicky}} - 0.05$. This should make these curves directly comparable with the other results in the b_J band. Both the Moore et al. and Marinoni et al. studies probe smaller volumes than in the 2PIGG case, so cosmic variance may be partly responsible for the lower abundance of $\lesssim 10^{11} h^{-2} L_\odot$ groups found in these earlier studies. Also, the group-finder used by Marinoni et al. places a higher fraction of galaxies into groups, so one might expect that fewer isolated galaxies would remain, yielding fewer low luminosity groups.

5 GROUP MASS-TO-LIGHT RATIOS

By comparing, at a fixed abundance, the measured cumulative group luminosity function with a mass function motivated by numerical simulations of a CDM model, it is possible to determine the mass-to-light ratio down to groups that contain only a single visible galaxy in the 2dFGRS. This method (see Marinoni & Hudson 2002, MH02) is shown schematically in Fig. 11, where the mass-to-light ratio gives the mapping from the cumulative luminosity function to the cumulative mass function. An assumption of this method is that the group mass varies monotonically with luminosity, so that this mapping is unique. Fig. 11 shows the importance of the choice of mass function. For instance, the Press & Schechter (1974) formula underestimates the abundance of the largest clusters and overestimates that of Local Group-sized objects. This overabundance would produce mass-to-light ratios for small groups that are too high by ~ 50 per cent.

This is an indirect, model-dependent measurement of the mass-to-light ratio, because the mass function shape and amplitude are assumed to be of a particular form, rather

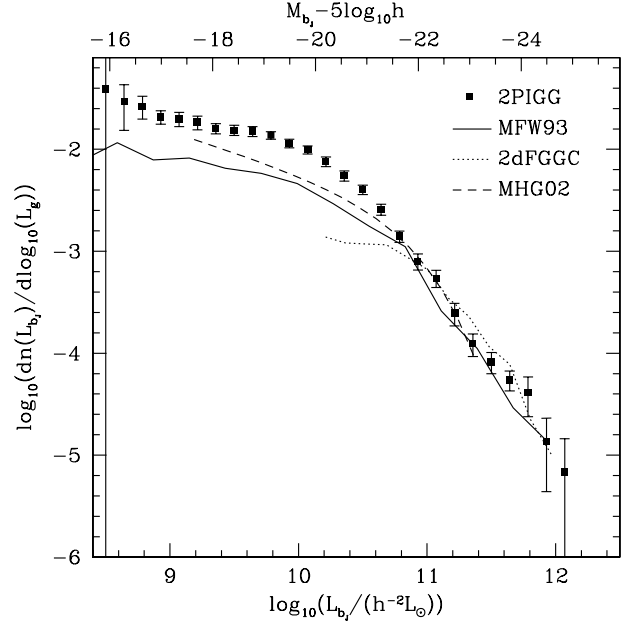


Figure 10. The abundance of groups as a function of their total b_J -band luminosity. The points show the group luminosity function found using the 2PIGG catalogue out to $z = 0.07$, whereas the lines show the results of Moore, Frenk & White (1993, solid), Marinoni, Hudson & Giuricin (2002, dashed) and Martínez et al. (2002, dotted).

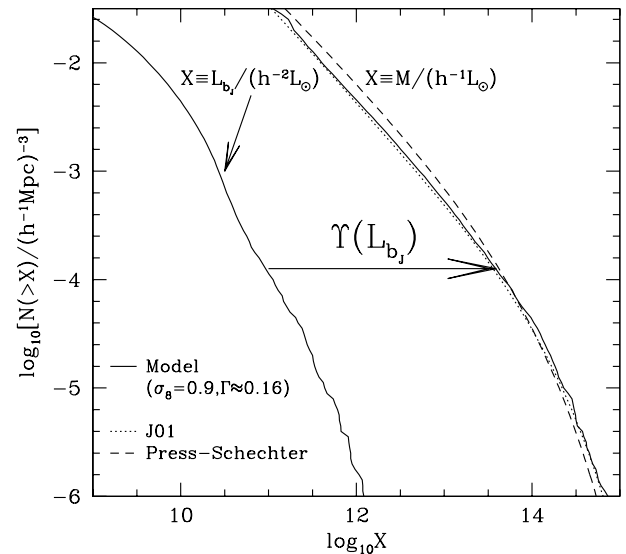


Figure 11. Cumulative group abundances as functions of both mass and luminosity in the simulation model. The quantity X on the horizontal axis, is either the group b_J -band luminosity in $h^{-2} L_\odot$ or the group mass in $h^{-1} M_\odot$. A dotted line shows the J01 fit to the mass function, whereas the dashed line is the corresponding Press-Schechter curve. The horizontal distance with an arrow represents the inferred group mass-to-light ratio for groups with a luminosity equal to $10^{11} h^{-2} L_\odot$.

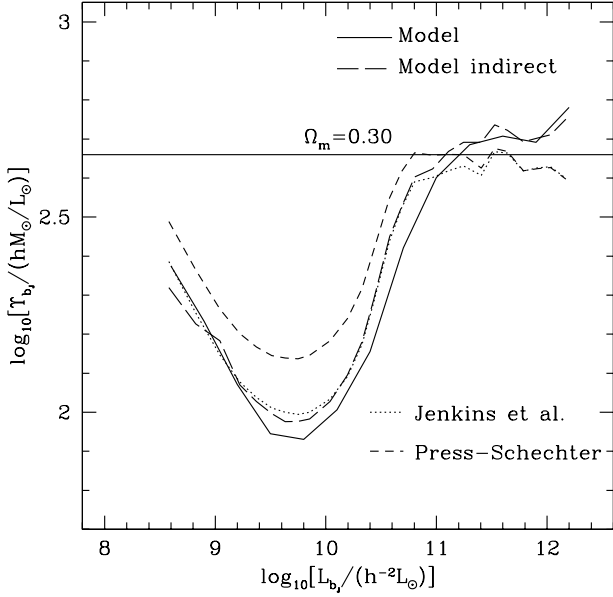


Figure 12. Model mass-to-light ratios as functions of group luminosity. The solid curve traces the median mass-to-light ratio in bins of group luminosity, whereas the long dashed line represents the function required to map the model group luminosity function to the model group mass function. If, instead of using the actual group mass function from the simulation, the J01 or Press-Schechter formulae are used, then the dotted and short dashed curves result.

than being directly measured. However, with this method one can probe to smaller group sizes, where group luminosities are still well-defined but the masses are difficult to measure. The uncertainty associated with the accuracy of the adopted mass function includes a non-negligible contribution from uncertainty in the value of σ_8 for the real Universe. As discussed in Section 3, the abundance of such clusters depends very sensitively upon σ_8 . Consequently, the mass-to-light ratios inferred from this method for these large objects will suffer from this uncertainty. However, for smaller groups, this effect is minor, and the mass function is quite robust to changes in σ_8 . Thus, this method for measuring the mass-to-light ratio is complementary to the direct measurement technique, which is most effective for the larger systems that have enough galaxies to allow an accurate mass estimation.

It is worth noting that the mass-to-light ratio as a function of group luminosity obtained by matching abundances is not the same as the median mass-to-light ratio of groups in each particular luminosity bin. This is because there is some scatter in the group masses at each group luminosity. However, the difference between these two mass-to-light ratios in the model can be seen in Fig. 12 to be small. Also shown are the results of inferring the mass-to-light ratio assuming the J01 and Press-Schechter mass functions rather than using the actual mass function. This illustrates the 50 per cent overestimation for small haloes mentioned in the discussion of the preceding figure. The J01 mass function is used throughout the rest of this paper.

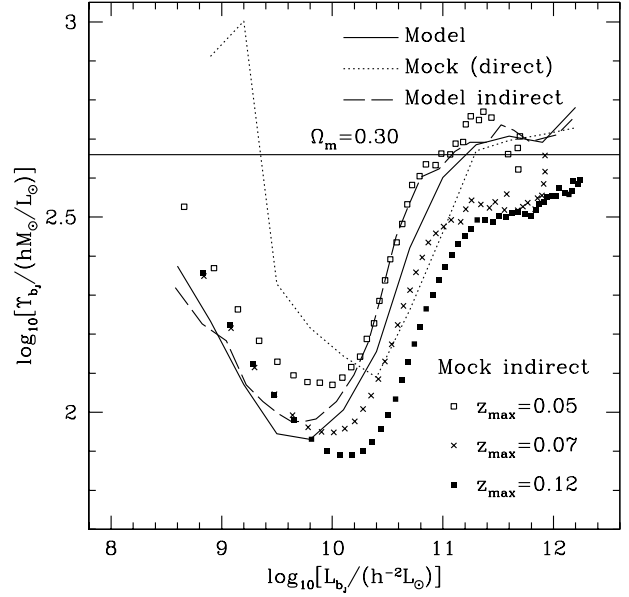


Figure 13. The recovery of the mass-to-light ratio as a function of group luminosity. The dotted curve traces the median mass-to-light ratio recovered from the mock catalogue using the dynamically inferred masses. This is the attempt to recover the model represented by the solid curve. The three sets of points show the mass-to-light ratio inferred from different sets of mock groups using the abundance-matching technique, and are attempts to measure the long-dashed curve of the model.

5.1 Results

The systematic errors in the recovery of the group luminosity function alluded to in Section 4 impact significantly upon the inferred variation of the group mass-to-light ratio. Fig. 13 shows how changing the maximum redshift of the mock group sample used to measure the luminosity function affects the results. For the largest groups, the mass-to-light ratio drops with increasing z_{\max} , as the abundance of clusters becomes more overestimated because of increasing contamination by interlopers and larger corrections for luminosity in galaxies beneath the flux limit. For groups with $L \lesssim 10^{10} h^{-2} L_{\odot}$ however, the volume probed is smaller and the errors associated with the correction from observed to total group luminosity are smaller. Consequently, the group luminosity functions are less dependent upon z_{\max} . The direct method for inferring the group mass-to-light ratio becomes significantly biased for $L \lesssim 10^{10} h^{-2} L_{\odot}$, so this group luminosity is an appropriate value at which to switch between the direct and indirect methods. In this way, the ‘corrected’ mass-to-light ratio can be recovered over almost four orders of magnitude in group luminosity. For $L > 10^{10} h^{-2} L_{\odot}$ the appropriate correction factor is the difference between the directly recovered curve (dotted) in Fig. 13 and the model curve (solid). For $L < 10^{10} h^{-2} L_{\odot}$ the correction factor is chosen to be the difference between the crosses and the model shown by the solid curve, so that the final ‘corrected’ curve provides an estimate of the typical mass-to-light ratio as a function of group luminosity.

The uncorrected results for the 2PIGG groups are shown in Fig. 14 and compared with those of MH02. As for

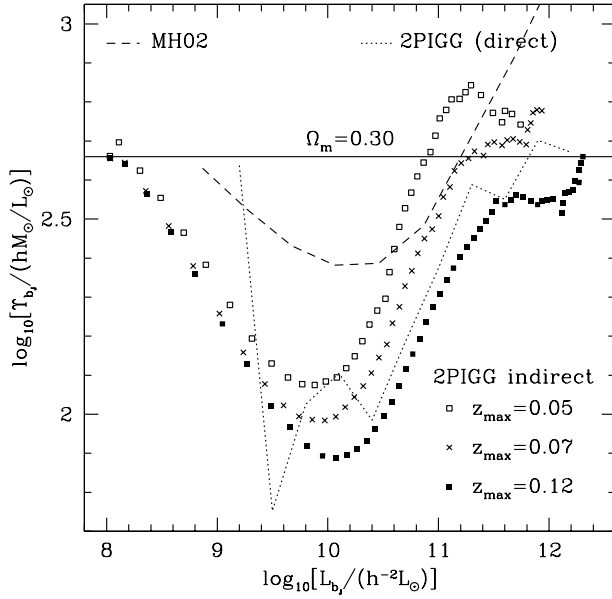


Figure 14. The recovery of the mass-to-light ratio as a function of group luminosity for the 2PIGG sample. The dotted curve traces the median mass-to-light ratio recovered using the dynamically inferred masses. The three sets of points show the mass-to-light ratio variation inferred from different sets of 2PIGG groups using the abundance-matching technique. A dashed line shows the results of Marinoni & Hudson (2002) from the NOG sample of galaxy groups.

the mock catalogues, the systematic differences between the different z_{\max} samples are evident for the bigger groups. The increasing overestimation of the group luminosity function, as z_{\max} increases, gives rise to decreasing inferred mass-to-light ratios. Note that the inferred mass-to-light ratio for the smallest groups is comparable with that measured directly for the clusters.

It is apparent that the 2PIGG results are somewhat different from those of MH02. This discrepancy arises for two main reasons. For the small groups, MH02 use the Press-Schechter formula for the mass function. As was seen in Fig. 13, this leads to an overestimation of the mass-to-light ratio of small groups by ~ 25 per cent (this, of course, assumes that the underlying mass function is that appropriate for Λ CDM). This difference is compounded at $L_{b,j} < 10^{10.6} h^{-2} L_{\odot}$ by the different group luminosity functions measured from the 2PIGG and NOG samples, as was shown in Fig. 10. As the NOG sample contains a lower abundance of groups at $L \lesssim 10^{10.6} h^{-2} L_{\odot}$, the inferred mass-to-light ratio is larger than for the 2PIGG sample. Note that the MH02 results in Fig. 14 differ from those plotted in figure 15 by Eke et al. (2004b), because they did not use the appropriate waveband correction.

Having calibrated the biases introduced by the two methods to measure group mass-to-light ratios with the mock catalogues, it is now possible to ‘correct’ the 2PIGG results in Fig. 14. Using the $z_{\max} = 0.07$ data for the indirect mass-to-light ratio measurement below $L = 10^{10} h^{-2} L_{\odot}$ yields the results shown in Fig. 15. The errors on the indirectly measured points come from the scatter between 22

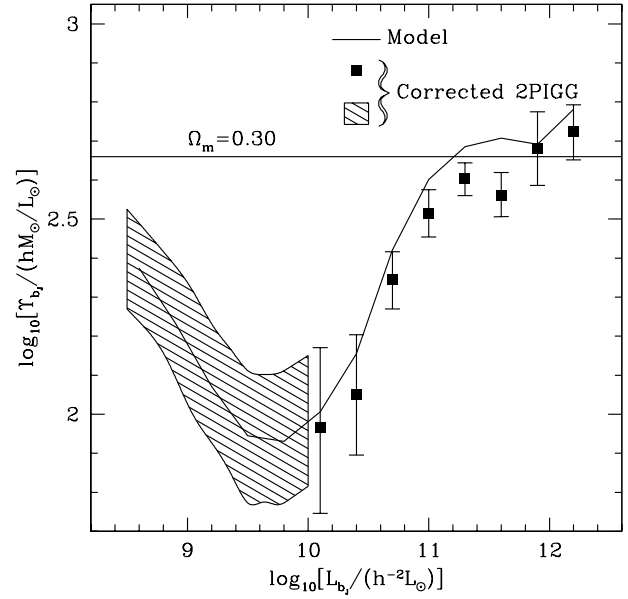


Figure 15. The ‘corrected’ mass-to-light ratio as a function of group luminosity for the 2PIGG sample. The error bars include the statistical errors added in quadrature to the uncertainty in the systematic shift applied to ‘correct’ the measurements. Directly measured mass-to-light ratios are shown with points, whereas those inferred assuming that the global halo mass function is given by the fitting function of J01 are shown by the shaded region.

mock catalogues made from the Hubble Volume simulation, added in quadrature to the uncertainty in the correction factor. For the $L > 10^{10} h^{-2} L_{\odot}$ results, the error bars show the statistical uncertainty in the raw mass-to-light ratio added in quadrature to the uncertainty in the correction factor. The uncertainties in the correction factors are calculated by taking eight different mock catalogues with different σ_8 values and semi-analytical schemes, and finding the scatter between the corrections.

The corrected mass-to-light ratio variation with luminosity for the 2PIGGs shows a plateau at cluster masses, a decrease to a minimum at $L \sim 10^{10} h^{-2} L_{\odot}$, and an increase for smaller groups. The value of the halo mass at this minimum is $\sim 10^{12} h^{-1} M_{\odot}$, which agrees well with the weak lensing analysis of Hoekstra, Yee & Gladders (2004). They found a halo of this luminosity to have $M_{200} = (8.4 \pm 0.7 \pm 0.4) \times 10^{11} h^{-1} M_{\odot}$, which should be increased by ~ 20 per cent to compare with the halo mass definition used here. It is reassuring that these two completely different methods show such consistency.

One might wonder how surprising it is that the corrected, recovered mass-to-light variation looks so similar to that in the model for $L < 10^{10} h^{-2} L_{\odot}$, where the masses of the 2PIGGs are not directly measured. After all, the model mass function has been assumed to be appropriate for the real Universe, and the galaxy luminosity function in the model has been scaled so as to match that of the 2dFGRS. The only possibility for the corrected 2PIGG results to differ from the model in Fig. 15 is if the group luminosity functions differ, despite the identical global galaxy luminosity functions. Thus, the measurement of an increase

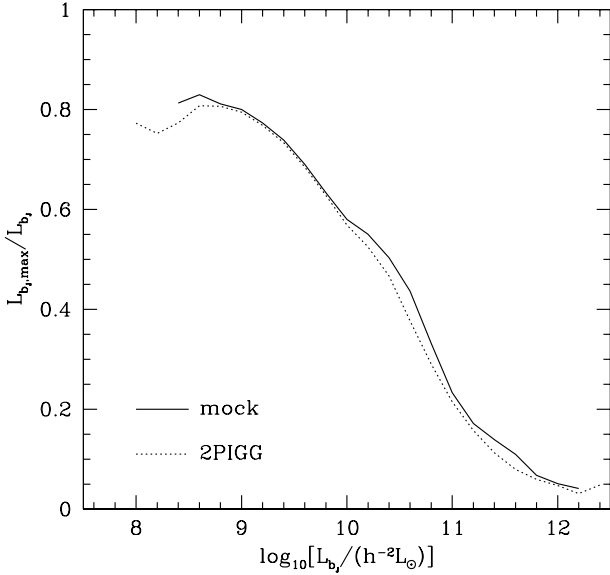


Figure 16. The ratio of the median brightest galaxy luminosity to the total group luminosity as a function of luminosity for the mock groups and 2PIGGs, shown with solid and dotted lines respectively.

in 2PIGG mass-to-light ratio as group size decreases from $L \sim 10^{10} h^{-2} L_{\odot}$ is, if not inevitable, to be expected merely from the fact that the faint end slope of the galaxy luminosity function is flatter than that of the Λ CDM mass function at low masses. The extra information available here comes from the fact that the group luminosity function is tracing the same structures probed with the mass function measurements. Consequently, the normalisation of the mass-to-light ratio is not predetermined but, in fact, recovered in addition to the variation with group size.

6 THE TULLY-FISHER RELATION

The results in Fig. 15 show how the typical halo mass varies with halo luminosity. For a particular definition of a halo, one can convert this to a relation between the halo circular speed and the halo luminosity via

$$L_{b,J} = \left(\frac{3}{4\pi\Delta\rho_{\text{crit}}} \right)^{\frac{1}{2}} \frac{1}{\Upsilon G^{\frac{3}{2}}} v_c^3, \quad (6.1)$$

where $\Delta\rho_{\text{crit}}$ represents the mean enclosed density of the halo, taken to be 100 times the critical value. (Note that this value is not exact because the identification of the groups is done using a FOF algorithm, rather than growing a sphere out to a particular density contrast.) This relation is reminiscent of the Tully-Fisher relation between galaxy luminosity and rotation speed at the edge of the visible galaxy. For low luminosity systems, a central bright galaxy usually dominates the total group luminosity, so the galaxy and group luminosities are likely to be quite similar. Fig. 16 shows the median ratio of the brightest galaxy to total group luminosity, as a function of total group luminosity. The mock and

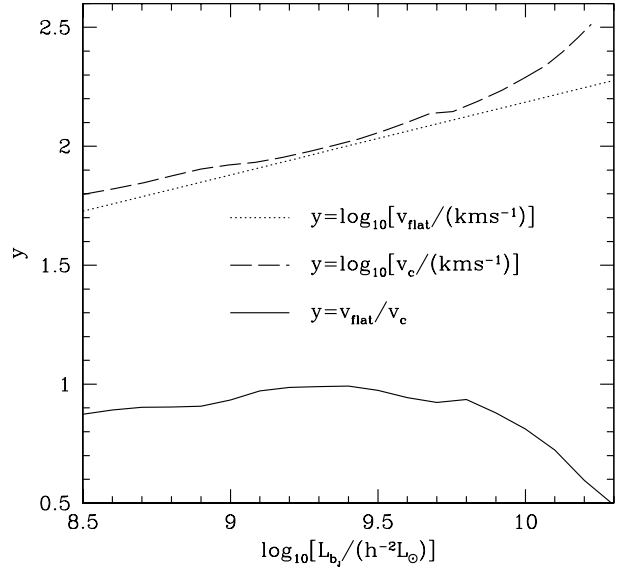


Figure 17. The galaxy rotation speed, v_{flat} , and inferred halo circular speed, v_c , as functions of blue luminosity. For the galaxy rotation speed curve (dotted line), the luminosity is that of the galaxy, according to the Tully-Fisher relation of Bell and de Jong (2001). The luminosity for the dashed curve is the total group luminosity multiplied by the ratio shown in Fig. 16 to convert it to the typical luminosity of the brightest galaxy in each halo. The solid line shows the ratio of these two velocities as a function of primary galaxy luminosity.

2PIGG curves are very similar, with the main difference being that the brightest galaxy in the bigger mock groups typically contains a slightly higher fraction of the total group luminosity than in the 2PIGGs.

If one were to apply the median shift of Fig. 16 to convert the group luminosity to the typical luminosity of the brightest contained galaxy, then equation (6.1) could relate galaxy luminosity to halo circular speed at the virial radius. Then, one might reasonably ask, given the Tully-Fisher relation and the results in Fig. 15, what is the relationship between the galaxy rotation speed and the halo circular speed for galaxies with $L \lesssim 10^{10} h^{-2} L_{\odot}$? The answer to this question is contained in Fig. 17. The B -band Tully-Fisher relation of Bell & de Jong (2001) has been converted to b_J , and is shown with a dotted line. Note that these authors advocate the use of v_{flat} to characterise the velocity derived from the galaxy rotation curve. The dashed curve shows the halo circular velocity from equation (6.1) as a function of luminosity (ie the group luminosity multiplied by the factor shown in Fig. 16 to convert it to a galaxy luminosity). A solid line traces the ratio of v_{flat} to v_c . How should this figure be interpreted? If one considers a galaxy with $L_{b,J} \sim 10^{10} h^{-2} L_{\odot}$, then the Tully-Fisher relation of Bell & de Jong gives $v_{\text{flat}} \sim 160 \text{ km s}^{-1}$, whereas the abundance matching method implies that it typically lives in a halo with circular speed $\sim 200 \text{ km s}^{-1}$. For less luminous galaxies, these two velocities become more similar, so that the flat part of the galaxy rotation curve corresponds to a

speed that is approximately the same as the circular velocity of the host halo.

The suggestion that the galaxy rotation speed is similar to the halo circular velocity is broadly in accord with the results for the *I*-band Tully-Fisher relation in the semi-analytical galaxy formation models of Cole et al. (2000) and Croton et al. 2005. They found that the galaxy luminosity function and the Tully-Fisher relation could be matched simultaneously when the galaxy rotation speed was assumed to equal the halo circular velocity. However, one would expect as baryons concentrate in the centres of galaxy-sized potential wells, they would drag in dark matter, leading to galaxy rotation speeds that are a few tens of per cent larger than the halo circular velocity. In this case, the Tully-Fisher relation is no longer reproduced by the model. Similar conclusions have been drawn from hydrodynamical simulations of galaxy formation by Navarro & Steinmetz (2000) and Eke, Navarro & Steinmetz (2001), and also from the analysis of de Jong et al. (2004).

It is possible that the comparison above could be misleading; perhaps the galaxies included in Tully-Fisher samples are atypical. If the observed set of galaxies lie in either unusually luminous or unusually low concentration haloes, then this might reconcile the apparent discrepancy between the low observed rotation speeds and the higher expected values. For example, the semi-analytical model behind the mock catalogues used in this work predicts that the distribution of masses of haloes with $L \sim 10^{10} h^{-2} L_{\odot}$ has a 1σ scatter that equates to ~ 20 per cent in halo circular speed. If, for some reason, the galaxies selected in the Tully-Fisher measurements lie in the less massive haloes at that particular luminosity, then this could have a very significant impact in reducing the dark matter contribution to the observed rotation curves. Similarly, if typical Tully-Fisher galaxies happen to lie in atypically unconcentrated haloes, then the dark matter contribution to the observed rotation curves would again be reduced.

7 CONCLUSIONS

The 2PIGG catalogue has been used to measure the mass and luminosity functions of groups and clusters. By combining the measured abundance of clusters as a function of luminosity, with a typical mass-to-light ratio, the cluster mass function is measured more accurately than by using the dynamically-inferred masses directly. After removing a bias due to measurement errors in the abundance, using that found in mock catalogues constructed from Λ CDM N-body simulations, the 2PIGG mass function implies that $\sigma_8 = 0.25 \Omega_m^{-0.92-4.5(\Omega_m-0.22)^2}$ for $0.18 \leq \Omega_m \leq 0.50$. While the statistical uncertainty on this value is around 10 per cent, the systematic correction that has been applied is closer to 20 per cent. The uncertainty in this correction, coupled with the systematic uncertainty in the normalisation of the estimated cluster masses (the value of A in equation 2.1), currently limits the precision of this determination of σ_8 to ~ 20 per cent. To decrease this uncertainty significantly would require a more detailed understanding of how the observed galaxies populate the underlying dark matter haloes.

The group luminosity function is in good agreement

with previous studies for groups with total b_J -band luminosity exceeding $\sim 4 \times 10^{10} h^{-2} L_{\odot}$. At lower luminosities, the abundance of 2PIGGs is somewhat larger than has previously been found from smaller samples. Matching this abundance to that of haloes of a given mass in Λ CDM simulations gives the mass-to-light ratio as a function of group size. This indirect method combined with the direct estimates of Eke et al. (2004b) at higher luminosities allows the recovery of the variation of the group mass-to-light ratio over almost four orders of magnitude in group luminosity. The resulting function has a minimum value of $\sim 100 h M_{\odot}/L_{\odot}$ at group luminosity $L_{b_J} \sim 5 \times 10^9 h^{-2} L_{\odot}$. Finally, the group mass-to-light ratio was used to infer the halo circular speed as a function of group luminosity. Comparison to the observed Tully-Fisher relation for galaxies suggests that, at a given galaxy luminosity, the observed rotation speed is similar to the typical halo circular speed.

The dependence of the group mass-to-light ratio on group luminosity provides a key test of various feedback processes invoked in models of galaxy formation (Benson et al. 2000; Benson et al. 2003; Croton et al. 2005). The agreement between the indirect determination at low luminosities presented in this paper and the results of the semi-analytical Λ CDM model assumed in the construction of the mock catalogues is encouraging. A direct determination based, for example, on a deeper redshift survey is desirable.

ACKNOWLEDGMENTS

We would like to thank Christian Marinoni for his very helpful comments concerning different wavebands. The Hubble Volume N-body simulation was carried out by the Virgo Supercomputing Consortium using computers based at the Computing Centre of the Max-Planck Society in Garching and at the Edinburgh parallel Computing Centre. VRE and CMB are Royal Society University Research Fellows. JFN acknowledges support from the Alexander von Humboldt and Leverhulme Foundations.

REFERENCES

- Allen S.W., Schmidt R.W., Fabian A.C., Ebeling H., 2003, MNRAS, 342, 287
- Bahcall N.A., Cen R., 1993, ApJ, 407, L49
- Bahcall N.A. et al., 2003, ApJ, 585, 182
- Bardeen J.M., Bond J.R., Kaiser N., Szalay A.S., 1986, ApJ, 304, 15
- Beers T.C., Flynn K., Gebhardt K., 1990, AJ, 100, 32
- Bell E.F., de Jong R.S., 2001, ApJ, 550, 212
- Benson A.J., Cole S., Frenk C.S., Baugh C.M., Lacey C.G., 2000, MNRAS, 311, 793
- Benson A.J., Bower R.G., Frenk C.S., Lacey C.G., Baugh C.M., Cole S., 2003, ApJ, 599, 38
- Biviano A., Girardi M., Giuricin G., Mardirossian F., Mezzetti M., 1993, ApJ, 411, L13
- Brown M.L., Taylor A.N., Bacon D.J., Gray M.E., Dye S., Meisenheimer K., Wolf C., 2003, MNRAS, 341, 100
- Cole S., Aragon-Salamanca A., Frenk C.S., Navarro J.F., Zepf S.E., 1994, MNRAS, 271, 781
- Cole S., Lacey C.G., Baugh C.M., Frenk C.S., 2000, MNRAS, 319, 168
- Cole S. et al. (The 2dFGRS Team), 2005, MNRAS, 362, 505

- Colless M. et al. (The 2dFGRS Team), 2001, MNRAS, 328, 1039
 Croton D.J. et al. , 2005, MNRAS, submitted, (astro-ph/0508046)
 Davis M., Efstathiou G., Frenk C.S., White S.D.M., 1985, ApJ, 292, 371
 de Jong R.S., Kassin S., Bell E.F., Courteau S., 2004, IAUS, 220, 281
 Eke V.R., Cole S., Frenk C.S., 1996, MNRAS, 282, 263
 Eke V.R., Navarro J.F., Steinmetz M., 2001, ApJ, 554, 114
 Eke V.R. et al. (The 2dFGRS Team), 2004a, MNRAS, 348, 866
 Eke V.R. et al. (The 2dFGRS Team), 2004b, MNRAS, 355, 769
 Evrard A.E., MacFarland T.J., Couchman H.M.P., Colberg J.M., Yoshida N., White S.D.M., Jenkins A., Frenk C.S., Pearce F.R., Peacock J.A., Thomas P.A., 2002, ApJ, 573, 7
 Frenk C.S., White S.D.M., Efstathiou G., Davis M., 1990, ApJ, 351, 10
 Girardi M., Borgani S., Giuricin G., Mardirossian F., Mezzetti M., 1998, ApJ, 506, 45
 Hawkins E. et al. (The 2dFGRS Team), 2003, MNRAS, 346, 78
 Henry J.P., 2004, ApJ, 609, 603
 Heyl J.S., Cole S., Frenk C.S., Navarro J.F., 1995, MNRAS, 274, 755
 Heymans C. et al., 2005, MNRAS, 361, 160
 Hoekstra H., Yee H.K.C., Gladders M.D., 2004, ApJ, 606, 67
 Ikebe Y., Reiprich T.H., Böhringer H., Tanaka Y., Kitayama T., 2002, A&A, 383, 773
 Jenkins A., et al., 1998, ApJ, 499, 20
 Jenkins A., Frenk C.S., White S.D.M., Colberg J.M., Cole S., Evrard A.E., Couchman H.M.P., Yoshida N., 2001, MNRAS, 321, 372
 Kauffmann G., White S.D.M., Guiderdoni B., 1993, MNRAS, 264, 201
 Marinoni C., Hudson M.J., Giuricin G., 2002, ApJ, 569, 91
 Marinoni C., Hudson M.J., 2002, ApJ, 569, 101
 Martínez H.J., Zandivarez A., Merchán M.E., Domínguez M.J.L., 2002, MNRAS, 337, 1441
 Massey R., Refregier A., Bacon D.J., Ellis R., Brown M.L., 2005, MNRAS, 359, 1277
 Moore B., Frenk C.S., White S.D.M., 1993, MNRAS, 261, 827
 Navarro J.F., Steinmetz M., 2000, ApJ, 538, 477
 Norberg P. et al. , 2002, MNRAS, 336, 907
 Peebles P.J.E., Daly R.A., Juskiewicz R., 1989, ApJ, 347, 563
 Pierpaoli E., Scott D., White M., 2001, MNRAS, 325, 77
 Pierpaoli E., Borgani S., Scott D., White M., 2003, MNRAS, 342, 163
 Pisani A., Ramella M., Geller M.J., 2003, AJ, 126, 1677
 Press W.H., Schechter P., 1974, ApJ, 187, 425
 Reiprich T.H., Böhringer H., 2002, ApJ, 567, 716
 Rhodes J., Refregier A., Collins N.R., Gardner J.P., Groth E.J., Hill R.S., 2004, ApJ, 605, 29
 Sanchez A.G., Baugh C.M., Percival W.J., Padilla N.D., Cole S., Frenk C.S., Norberg P., 2005, MNRAS, submitted (astro-ph/0507583)
 Seljak U., 2002, MNRAS, 337, 769
 Schuecker P., Böhringer H., Collins C.A., Guzzo L., 2003, A&A, 398, 867
 Sugiyama N., 1995, ApJS, 100, 281
 Tully R.B., Fisher J.R., 1977, A&A, 54, 661
 van den Bosch F.C., Yang X., Mo H.J., 2003, MNRAS, 340, 771
 van Waerbeke L., Mellier Y., Hoekstra H., 2005, A&A, 429, 75
 Viana P.T.P., Liddle A.R., 1996, MNRAS, 281, 323
 Viana P.T.P., Nichol R.C., Liddle A.R., 2002, ApJ, 569, L75
 Viana P.T.P., Kay S.T., Liddle A.R., Muanwong O., Thomas P.A., 2003, MNRAS, 346, 319
 White S.D.M., Efstathiou G., Frenk C.S., 1993, MNRAS, 262, 1023